photonics

MDPI

Communication

Enhancing the Self-Healing Ability of a Partially Coherent Airy Beam via Fourier Processing: Numerical Investigation

Yuefeng Zhao [1,2], Yinghe Wang [1,2], Qian Chen [1,2], Pujuan Ma [1,2], Yangjian Cai [1,2,*] and Chunhao Liang [1,2,*]

[1] Shandong Provincial Engineering and Technical Center of Light Manipulation & Shandong Provincial Key Laboratory of Optics and Photonic Devices, School of Physics and Electronics, Shandong Normal University, Jinan 250014, China
[2] Collaborative Innovation Center of Light Manipulations and Applications, Shandong Normal University, Jinan 250358, China
* Correspondence: yangjian_cai@163.com (Y.C.); chunhaoliang@sdnu.edu.cn (C.L.)

Abstract: Almost all of the beams under propagation are believed to suffer severe distortion when the source coherence deteriorates, due to the optical diffraction. This implies that low-coherence beams have poor self-healing ability, but were found to be robust against the turbulence, distortion, scattering, etc. In this letter, we first prove numerically that partially coherent Airy beams (PCABs), generated via Fourier processing, have better self-healing ability than that of conventional fully coherent Airy beams. Moreover, as the source coherence deteriorates and the propagation distance increases, the self-healing ability is found to increase. We believe that such PCABs may find Airy beam-related applications in adverse environments, such as particle trapping in biological tissues.

Keywords: Airy beam; partially coherent beam; self-healing; Fourier processing

Citation: Zhao, Y.; Wang, Y.; Chen, Q.; Ma, P.; Cai, Y.; Liang, C. Enhancing the Self-Healing Ability of a Partially Coherent Airy Beam via Fourier Processing: Numerical Investigation. *Photonics* **2023**, *10*, 143. https://doi.org/10.3390/photonics10020143

Received: 15 December 2022
Revised: 23 January 2023
Accepted: 26 January 2023
Published: 30 January 2023

1. Introduction

Optical coherence, an intrinsic property of light beams, determines the interference effect. With the establishment of optical coherence theory [1], particularly regarding the sufficient and necessary conditions for customizing genuine partially coherent beams (PCBs) [2,3], there is a wealth of literature on the generation, propagation, and applications of such beams [4–20]. The van Critter–Zernike theorem and mode superposition principle are widely used to produce PCBs with prescribed properties. PCBs propagating in free space, turbulent atmospheres/oceans/tissues, and nonlinear media, or scattered by a diffuser have been studied in depth [4–12]. The results demonstrate that optical coherence determines the behavior of PCBs and renders them robust against turbulence, nonlinearity, and scattering. Based on the inherent characteristics and unique advantages of PCBs, they have found applications in optical communication, particle trapping, super-resolution images, and speckle-free images [13–17]. In particular, our group recently proposed an encryption technique based on optical coherence [18]. Optical information can be decrypted from the degree of coherence (DOC) of the PCB using the matched key. The DOC, as a second-order statistical parameter, cannot be accessed by the human eye or any camera. Hence, this optical coherence encryption technique is highly secure. Furthermore, we proposed a far-field optical imaging technique wherein the DOC was treated as an information carrier [19,20]. The results demonstrated that it can be immune to obstacles and turbulence.

Self-healing refers to the capacity of a beam obstructed by an opaque object to reconstruct itself after traveling a certain distance. This remarkable property enables a beam to negotiate adverse environments, such as scattering and medium inhomogeneity. Self-healing has sparked numerous related studies on fully and partially coherent beams [21–31]. Researchers have employed wave optics, geometric optics, energy flow, and other theories to fully explain the self-healing phenomenon [29–31]. Such a property would allow the application of fully and partially coherent beams in light microscopes, ghost imaging,

optical communication, optical imaging, among others [20,32–34]. Airy beams were first predicted as diffraction-free beams and observed by Siviloglou et al. in 2007 [35,36]. They possess self-healing attributes that can be described by Babinet's principle. In contrast to other diffraction-free beams, Airy beams exhibit self-accelerating properties, which can be interpreted using the principle of equivalence [37]. Consequently, Airy beams have attracted much attention in different areas, from fundamental science to real-world applications. Numerous studies have focused on the customization, propagation, and light–matter interaction of Airy beams, and they have found applications in super-resolution imaging, plasma channel generation, optical communications, and particle trapping [38–48]. Airy beams are not square integrable; hence, we must introduce an exponential aperture function to realize such beams in the laboratory. The truncated Airy beams maintain their shapes invariantly only for a certain distance, and their self-healing ability undoubtedly deteriorates. Moreover, it is well known that, as the source coherence deteriorates, a beam with finite energy readily suffers from shape distortion during propagation, owing to optical diffraction. This prompts a natural question: is it possible that a partially coherent Airy beam (PCAB) has a higher self-healing ability than that of a fully coherent one? If it is possible, this would prompt Airy beams to find more applications, especially in the adverse environments.

In this study, we explore the self-healing properties of PCABs generated via Fourier processing. It is found that the self-healing ability can be improved through Fourier processing and that the self-healing ability is further enhanced as the source coherence deteriorates.

2. Theory

First, we briefly introduce the generation of a PCAB via Fourier processing. This beam differs from the conventional PCAB. For the former, the DOC has an Airy-like profile, whereas for the latter, the DOC normally has a Gaussian distribution [40,42]. In the protocol presented in [40], Liu et al. used a modified 4f optical system to realize Fourier processing, as shown in the left part of Figure 1.

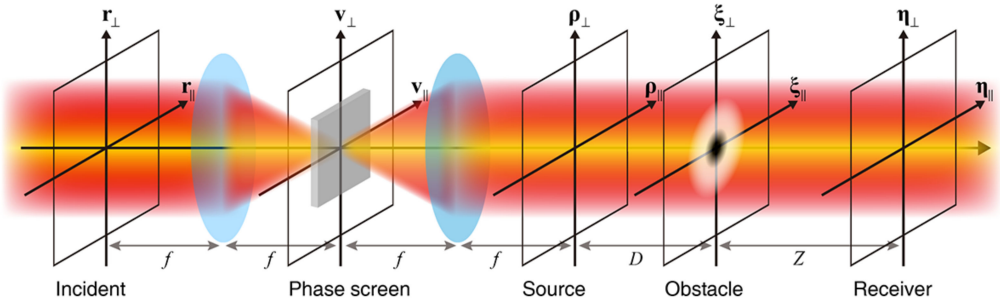

Figure 1. Schematic diagram for the generation of a PCAB via Fourier processing and study of its self-healing property. The system comprises two identical lenses with the focal length f, a phase screen, and one obstacle. All relevant planes and axes are indicated.

This system consisted of two identical thin lenses and a phase screen located in the spatial frequency plane. The front focal plane of the first lens and rear focal plane of the second lens were treated as the incident and source planes, respectively. The incident source for this optical system was a Gaussian Schell-model beam characterized by the following cross-spectral density function in the space–frequency domain.

$$W(\mathbf{r}_1, \mathbf{r}_2) = \exp\left(-\frac{\mathbf{r}_1^2 + \mathbf{r}_2^2}{4\omega_0^2}\right) \exp\left[-\frac{(\mathbf{r}_1 - \mathbf{r}_2)^2}{2\delta_0^2}\right], \tag{1}$$

where ω_0 and δ_0 denote the transverse beam and coherence widths, respectively. $\mathbf{r}_i = \left(\mathrm{r}_{\perp i}, \mathrm{r}_{\parallel i}\right), i = 1, 2$, is an arbitrary position vector in the incident plane. The adopted function for the phase screen is:

$$P(\mathbf{v}) = \exp\left\{-ik\left[(a\mathrm{v}_\perp)^3 + (a\mathrm{v}_\parallel)^3\right]\right\}, \tag{2}$$

where $k = 2\pi/\lambda$ denotes the wavenumber, λ is the wavelength, and a is a constant in unit of $\mathrm{m}^{-2/3}$. $\mathbf{v} = \left(\mathrm{v}_\perp, \mathrm{v}_\parallel\right)$ is an arbitrary position vector in the space–frequency plane. After Fourier processing, the Gaussian Schell-model beam becomes a PCAB in the source plane. Further details can be found in [40]. We now consider an opaque obstacle along the propagation path, as shown in the right part of Figure 1. We assume that the distances from the source plane to the obstacle plane and from the obstacle plane to the receiver plane are D and Z, respectively. The propagation evolution of PCBs can be studied using the Huygens–Fresnel integral principle. To clearly describe the entire self-healing process, we divided it into three steps. The first step is a PCAB propagating from the source plane to the front surface of the obstacle. With the aid of the Huygens–Fresnel integral principle, it is described by:

$$\begin{aligned} W_D(\xi_1, \xi_2) &= \tfrac{1}{\lambda^2 D^2} \exp\left[-\tfrac{ik}{2D}\left(\xi_1^2 - \xi_2^2\right)\right] \\ \times \iint W_0(\boldsymbol{\rho}_1, \boldsymbol{\rho}_2) &\exp\left[-\tfrac{ik}{2D}\left(\boldsymbol{\rho}_1^2 - \boldsymbol{\rho}_2^2\right) + \tfrac{ik}{D}\left(\boldsymbol{\rho}_1 \cdot \xi_1 - \boldsymbol{\rho}_2 \cdot \xi_2\right)\right] d^2\boldsymbol{\rho}_1 d^2\boldsymbol{\rho}_2, \end{aligned} \tag{3}$$

where $\boldsymbol{\rho}_i = \left(\rho_{\perp i}, \rho_{\parallel i}\right)$ and $\xi_i = \left(\xi_{\perp i}, \xi_{\parallel i}\right)$, $i = 1, 2$ are arbitrary position vectors in the source and obstacle planes, respectively. In the second step, the arriving beam is obstructed by an opaque obstacle, and the following equation is used to describe it:

$$W_D\prime(\xi_1, \xi_2) = \tau(\xi_1)\tau^*(\xi_2) W_D(\xi_1, \xi_2), \tag{4}$$

where $\tau(\xi)$ denotes the transmittance function of the obstacle. In the last step, the obstructed beam propagates further to the receiver plane. It is expressed as:

$$\begin{aligned} W_Z(\boldsymbol{\eta}_1, \boldsymbol{\eta}_2) &= \tfrac{1}{\lambda^2 Z^2} \exp\left[-\tfrac{ik}{2Z}\left(\boldsymbol{\eta}_1^2 - \boldsymbol{\eta}_2^2\right)\right] \\ \times \iint W_D\prime(\xi_1, \xi_2) &\exp\left[-\tfrac{ik}{2Z}\left(\xi_1^2 - \xi_2^2\right) + \tfrac{ik}{Z}\left(\xi_1 \cdot \boldsymbol{\eta}_1 - \xi_2 \cdot \boldsymbol{\eta}_2\right)\right] d^2\xi_1 d^2\xi_2. \end{aligned} \tag{5}$$

where $\boldsymbol{\eta}_i = \left(\eta_{\perp i}, \eta_{\parallel i}\right)$, $i = 1, 2$ is an arbitrary position vector in the receiver plane. If the obstacle is located in the source plane, that is D = 0 m, only the last two steps need to be performed. As suggested in [40], we can employ the complex screen method [49] to numerically simulate the entire process and achieve the intensity of the PCAB in the receiver plane.

When the intensity of the PCAB with or without the obstacle is achieved, we can use the similarity degree parameter to quantitatively describe the self-healing ability of the beam. The similarity degree is given in [22] by:

$$S = \frac{\left[\iint I_{wt}(\boldsymbol{\eta}) I_{ob}(\boldsymbol{\eta}) d^2\boldsymbol{\eta}\right]^2}{\iint |I_{wt}(\boldsymbol{\eta})|^2 d^2\boldsymbol{\eta} \iint |I_{ob}(\boldsymbol{\eta})|^2 d^2\boldsymbol{\eta}}. \tag{6}$$

The similarity degree, S, falls within the interval [0, 1]. $I_{wt}(\boldsymbol{\eta})$ and $I_{ob}(\boldsymbol{\eta})$ represent the intensity of the beams with and without the obstacle, respectively. The larger the S value,

the better the self-healing ability. In the following numerical simulation, we choose the inverted Gaussian function as an obstacle for simplicity:

$$\tau(\xi) = 1 - \exp\left(-\frac{\xi^2}{\sigma_0^2}\right), \tag{7}$$

where σ_0 characterizes the transverse width of the obstacle. The relevant parameters are given as $\lambda = 532$ nm, $f = 150$ mm, $a = 450\ m^{-2/3}$, $\omega_0 = 1$ mm, and $\sigma_0 = 5$ mm. Other parameters are discussed below.

3. Numerical Results

In this section, we use the above equations to explore the self-healing properties of PCABs obstructed by opaque obstacles. We consider two situations: in the first, the obstacle is located in the source plane, and in the second, the obstacle is located in the propagation path. The former is more common in the literature, and the latter has more practical significance.

Case 1: The Obstacle Is Located in the Source Plane

To visualize the entire process of the self-healing of PCABs, we show the intensity profiles of an obstructed beam at different distances during propagation. The results are shown in Figure 2, and the source coherence width is given by $\delta_0 = 1$mm. Figure 2a shows that the main peak of the PCAB is blocked by an opaque obstacle. The energy of the side lobes of the beam gradually flows toward the main peak with increasing propagation distance, as shown in Figure 2b,c. When the beam propagates further, the Airy pattern recovers well, as shown in Figure 2d,f. To investigate the effect of the source coherence on the self-healing of PCABs, we display the intensity profiles of the obstructed beam with different coherence widths δ_0 in the receiver plane Z = 160 m. It is worth noting that in the case of $\delta_0 = \infty$, shown in Figure 3a, the PCAB reduces to a conventional fully coherent Airy beam, as described in [40]. It is found that for the conventional fully coherent Airy beam, although the main peak recovers, the side lobes are deformed (there is a large dark area near the main peak). It is evident that, as the source coherence decreases, the main peak and side lobes gradually recover. Hence, we can infer that the self-healing ability of PCABs is better than that of conventional fully coherent Airy beams, and it is improved by decreasing the source coherence.

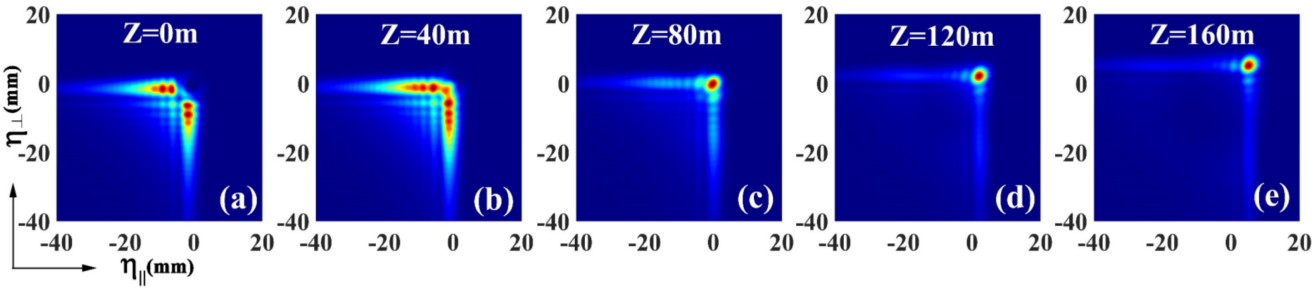

Figure 2. Density plots of the intensity distributions of a PCAB at the different propagation distances (**a**) Z = 0 m, (**b**) Z = 40 m, (**c**) Z = 80 m, (**d**) Z = 120 m, and (**e**) Z = 160 m during propagation. The beam is obstructed by an opaque obstacle in the source plane. The source coherence width is given by $\delta_0 = 1$ mm.

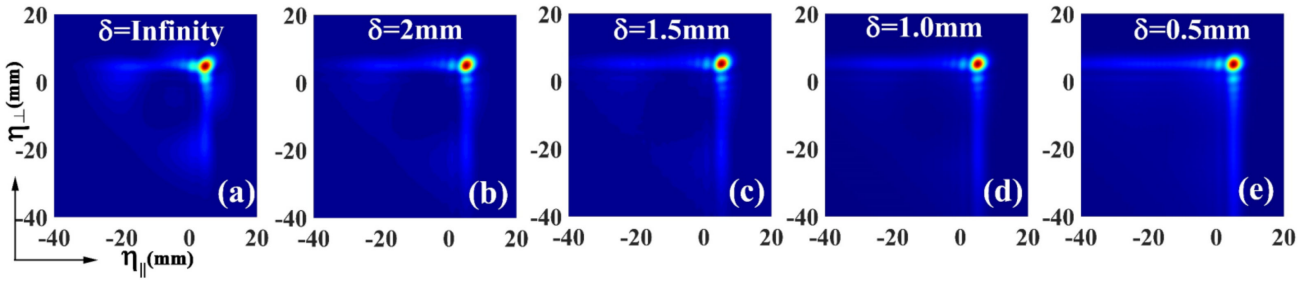

Figure 3. Density plots of the intensity distributions of (**a**) a conventional fully coherent Airy beam and (**b**–**e**) PCAB with different source coherence widths. The beam is obstructed by an opaque ob-stacle in the source plane, and the receiver plane is at Z = 160 m.

To quantitatively describe the self-healing ability of a PCAB, we use the similarity degree, defined by Equation (6), to investigate the effect of the source coherence and propagation distance Z on the self-healing property of the beam. We plot the similarity degree as a function of the coherence width δ_0 for different distances. The results are shown in Figure 4. The different colors, explained in the top-left corner, denote different propagation distances. As the source coherence deteriorates (δ_0 decreases from left to right in the plots), the similarity degree S increases, which implies that the obstructed PCAB gradually recovers. In particular, after $\delta_0 = 1$ mm, the similarity degree S increases rapidly, and reaches 0.904 when $\delta_0 = 0.25$ mm for the Z = 20 m curve. As described by coherence theory [1], if the coherence area is much larger than the beam spot area ($\delta_0^2 \gg \omega_0^2$), the partially coherent beam can be treated as a fully coherent beam. Hence, for $\delta_0^2 \gg \omega_0^2$, the similarity degree S value remains almost invariant at approximately 0.235. The similarity degree S ranges from 0.235 to 0.904 when we reduce the source coherence of a (quasi-) fully coherent Airy beam to that of a low-coherence Airy beam. This proves that the self-healing ability of the PCAB is effectively improved as the source coherence decreases, and that such a PCAB has a much better self-healing ability than the conventional fully coherent Airy beam. Furthermore, as shown by the left straight line (at $\delta_0 = 3.88$ mm) and annotation, the similarity degree S ranges from 0.144 to 0.235 when the propagation distance varies from Z = 5 to 20 m. This demonstrates that the self-healing ability of the beams increases with the propagation distance. This is also achieved in [22].

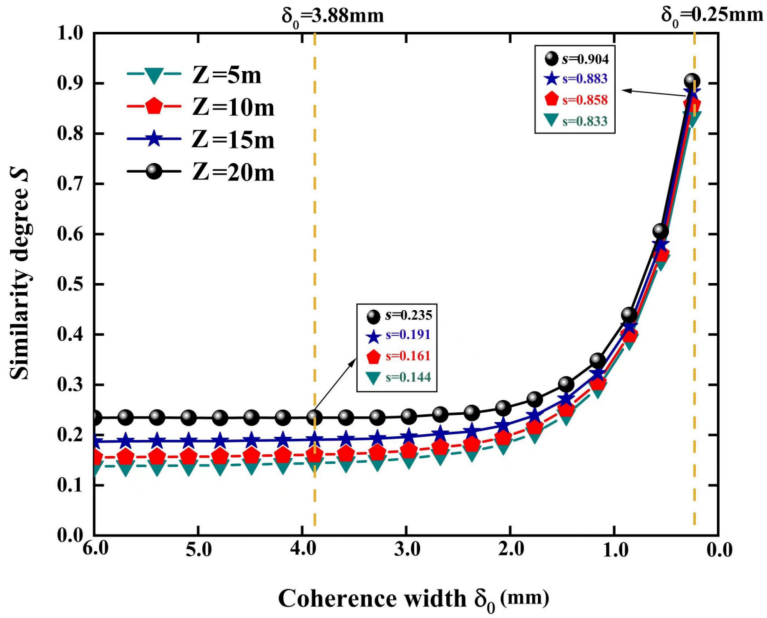

Figure 4. Similarity degree S of the PCAB as a function of the coherence width δ_0, for the different propagation distances. The different colors represent the different propagation distances.

Case 2: The Obstacle Is Located in the Propagation Path at D = 10 m

Next, we explore the self-healing property of the PCAB when the obstacle is located in the propagation path at D = 10 m. This case has more practical significance, such as a bird flying across the optical path of outdoor optical communication. First, we explore the intensity evolution of the obstructed propagating PCAB. The results shown in Figure 5 are almost the same as those in Figure 2. As the propagation distance increases, the blocked main peak of the beam gradually recovers and tends to stabilize. Furthermore, we focus on the effect of the source coherence on the self-healing ability of the beam, and the relevant results are displayed in Figure 6. The achieved results are almost the same as those in Case 1. For the conventional fully coherent Airy beam (see Figure 6a), although its main peak recovers, the side lobes are still highly deformed. We found that the entire PCAB recovers well as the source coherence deteriorates.

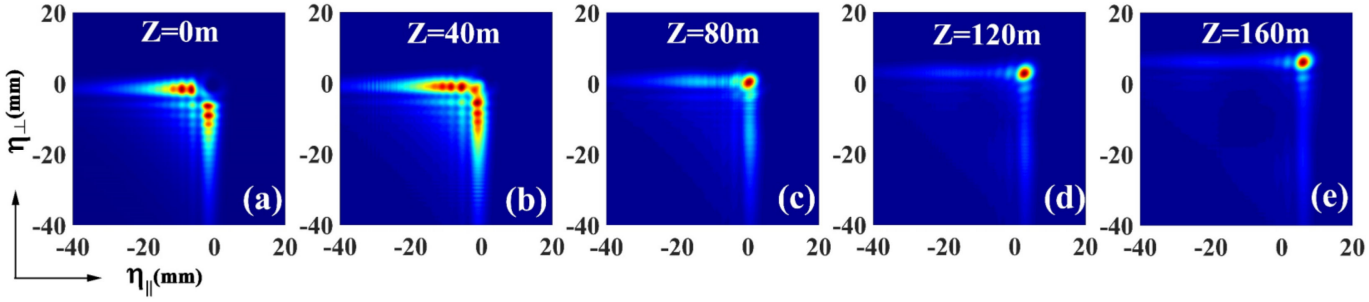

Figure 5. Density plots of the intensity distributions of a PCAB at the different propagation distances Z during propagation (**a**–**e**). The beam is obstructed by an opaque obstacle in the source plane. The source coherence width is $\delta_0 = 1$ mm.

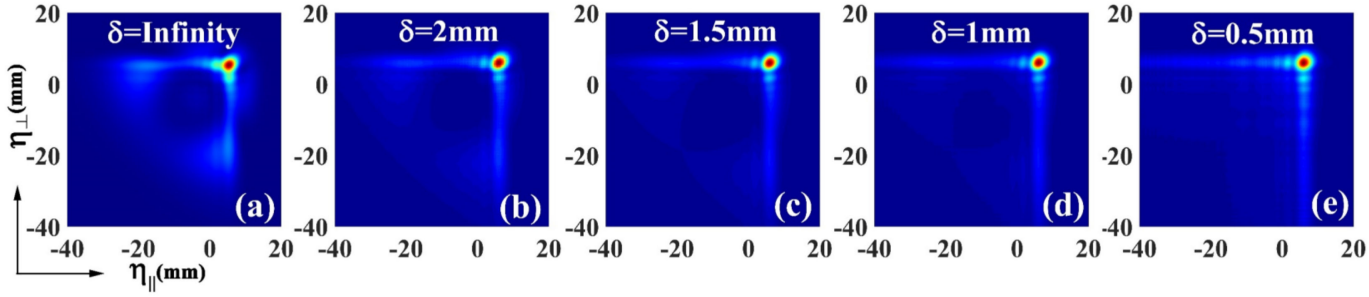

Figure 6. Density plots of the intensity distributions of (**a**) the fully coherent Airy beam and (**b**–**e**) PCABs for different source coherence widths. The beam is obstructed by an opaque obstacle in the source plane, and the receiver plane is at Z = 160 m.

Finally, we quantitatively describe the self-healing ability of the PCAB obstructed by an opaque obstacle at D = 10 m. The similarity degree curves are plotted in Figure 7 as a function of the coherence width δ_0 for different propagation distances Z. Each curve illustrates that the self-healing ability of the beam increases as the source coherence decreases. Taking the Z = 10 m case as an example, the (quasi-) fully coherent Airy beam has a similarity degree of S = 0.154, and the low-coherence Airy beam with $\delta_0 = 0.2$ mm has a similarity degree of S = 0.895. The self-healing ability of such a PCAB is significantly larger than that of the conventional fully coherent Airy beam, even with an obstacle in the propagation path. Likewise, for a fixed source coherence, the self-healing ability of the beam can be further enhanced with the propagation distance.

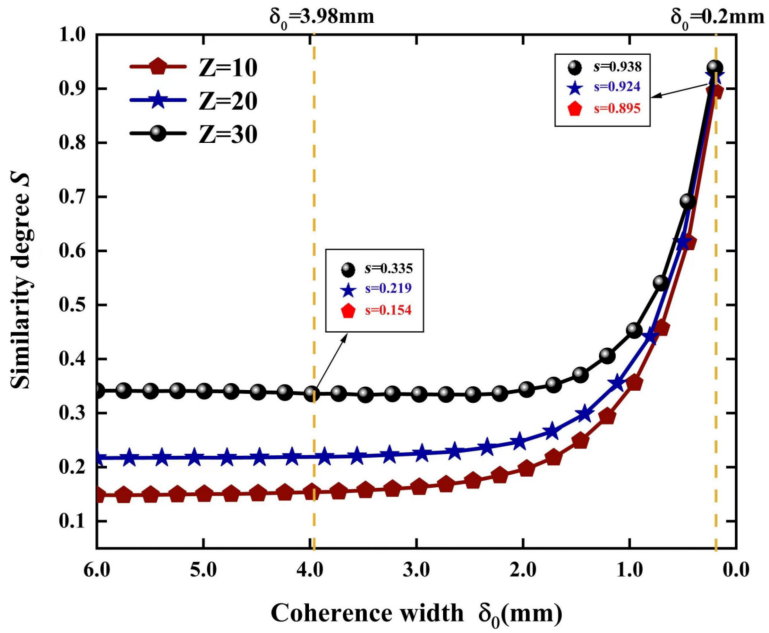

Figure 7. Similarity degree of the PCAB as a function of the coherence width δ_0, for different prop-agation distances. The different colors represent the different propagation distances.

4. Conclusions

In conclusion, we explored the self-healing properties of a PCAB proposed in [40]. We found that the self-healing ability of such a beam was much better than that of a conventional fully coherent Airy beam. Furthermore, its self-healing ability was enhanced as the source coherence deteriorated, in contrast to the conventional belief that a beam with lower coherence easily undergoes shape deformation and becomes less self-healable. The reason behind this is that the degree of coherence of such an Airy beam has an Airy-like profile, which causes it to propagates for a longer distance without distortion, i.e., better anti-diffraction ability [40]. The self-healing ability of the beam could be further improved by increasing the propagation distance. The above conclusions are valid for obstacles located in the source plane or propagation path. Finally, it is worth noting that our beam is partially coherent, and it is well known that a partially coherent beam is robust against turbulence, scattering, etc. Hence, we believe that our results provide constructive suggestions for the application of Airy beams in adverse environments.

Author Contributions: Conceptualization, C.L.; investigation, Y.Z. and Y.W.; methodology, P.M.; validation, Q.C.; software, Y.W. and Q.C.; writing—original draft preparation, Y.Z. and Y.W.; writing—review and editing, Y.C. and C.L.; funding acquisition, Y.C. and C.L.; project administration, Y.C. and Y.Z.; supervision, C.L. and Y.Z. All authors have read and agreed to the published version of the manuscript.

Funding: This research was funded by National Key Research and Development Program of China (Grant Nos. 2022YFA1404800 and 2019YFA0705000); National Natural Science Foundation of China (Grant Nos. 11974218, 12004220, 12004225, 12104264, 12192254, and 92250304); Regional Science and Technology Development Project of the Central Government (Grant No. YDZX20203700001766); China Postdoctoral Science Foundation (Grant Nos. 2020M672112, 2021T140425, and 2022T150392).

Institutional Review Board Statement: Not applicable.

Informed Consent Statement: Not applicable.

Data Availability Statement: The data presented in this study is available on request from the corresponding author.

Conflicts of Interest: The authors declare no conflict of interest.

References

1. Mandel, L.; Wolf, E. *Optical Coherence and Quantum Optics*; Cambridge University Press: Cambridge, UK, 1995.
2. Gori, F.; Santarsiero, M. Devising genuine spatial correlation functions. *Opt. Lett.* **2007**, *32*, 3531–3533. [CrossRef] [PubMed]
3. Gori, F.; Ramírez-Sánchez, V.; Santarsiero, M.; Shirai, T. On genuine cross-spectral density matrices. *J. Opt. A Pure Appl. Opt.* **2009**, *11*, 085706. [CrossRef]
4. Liang, C.; Wang, F.; Liu, X.; Cai, Y.; Korotkova, O. Experimental generation of cosine-Gaussian-correlated Schell-model beams with rectangular symmetry. *Opt. Lett.* **2014**, *39*, 769–772. [CrossRef] [PubMed]
5. Liang, C.; Liu, X.; Xu, Z.; Wang, F.; Wen, W.; Ponomarenko, S.A.; Cai, Y.; Ma, P. Perfect optical coherence lattices. *Appl. Phys. Lett.* **2021**, *119*, 131109. [CrossRef]
6. Wang, F.; Liu, X.; Cai, Y. Propagation of partially coherent beam in turbulent atmosphere: A review (invited review). *Prog. Electromagn. Res.* **2015**, *150*, 123–143. [CrossRef]
7. Xu, Z.; Liu, X.; Cai, Y.; Ponomarenko, S.A.; Liang, C. Structurally stable beams in the turbulent atmosphere: Dark and antidark beams on incoherent background. *J. Opt. Soc. Am. A* **2022**, *39*, C51–C57. [CrossRef]
8. Wang, H.; Ji, X.-L.; Deng, Y.; Li, X.-Q.; Yu, H. Theory of the quasi-steady-state self-focusing of partially coherent light pulses in nonlinear media. *Opt. Lett.* **2020**, *45*, 710–713. [CrossRef]
9. Wang, X.; Tang, J.; Wang, Y.; Liu, X.; Liang, C.; Zhao, L.; Hoenders, B.J.; Cai, Y.; Ma, P. Complex and phase screen methods for studying arbitrary genuine Schell-model partially coherent pulses in nonlinear media. *Opt. Express* **2022**, *30*, 24222–24231. [CrossRef]
10. Dong, Y.; Guo, L.; Liang, C.; Wang, F.; Cai, Y. Statistical properties of a partially coherent cylindrical vector beam in oceanic turbulence. *J. Opt. Soc. Am. A* **2015**, *32*, 894–901. [CrossRef]
11. Duan, M.; Du, J.; Zhao, H.; Zhang, X.; Gao, Y. The singularity of the partially coherent beam in biological tissue. *Results Phys.* **2022**, *43*, 106097.
12. Van Dijk, T.; Fischer, D.G.; Visser, T.D.; Wolf, E. Effects of spatial coherence on the angular distribution of radiant intensity generated by scattering on a sphere. *Phys. Rev. Lett.* **2010**, *104*, 173902. [CrossRef]
13. Lu, X.; Shao, Y.; Zhao, C.; Konijnenberg, S.; Zhu, X.; Tang, Y.; Cai, Y.; Urbach, H.P. Noniterative spatially partially coherent diffractive imaging using pinhole array mask. *Adv. Photon.* **2019**, *1*, 016005. [CrossRef]
14. Xu, Z.; Li, X.; Liu, X.; Ponomarenko, S.A.; Cai, Y.; Liang, C. Vortex preserving statistical optical beams. *Opt. Express* **2020**, *28*, 8475–8483. [CrossRef]
15. Redding, B.; Choma, M.A.; Cao, H. Speckle-free laser imaging using random laser illumination. *Nat. Photonics* **2012**, *6*, 355–359. [CrossRef]
16. Liang, C.; Wu, G.; Wang, F.; Li, W.; Cai, Y.; Ponomarenko, S.A. Overcoming the classical Rayleigh diffraction limit by controlling two-point correlations of partially coherent light sources. *Opt. Express* **2017**, *25*, 28352–28362. [CrossRef]
17. Liang, C.; Monfared, Y.E.; Liu, X.; Qi, B.; Wang, F.; Korotkova, O.; Cai, Y. Optimizing illumination's complex coherence state for overcoming Rayleigh's resolution limit. *Chin. Opt. Lett.* **2021**, *19*, 052601. [CrossRef]
18. Peng, D.; Huang, Z.; Liu, Y.; Chen, Y.; Wang, F.; Ponomarenko, S.A.; Cai, Y. Optical coherence encryption with structured random light. *PhotoniX* **2021**, *2*, 6. [CrossRef]
19. Liu, Y.; Chen, Y.; Wang, F.; Cai, Y.; Liang, C.; Korotkova, O. Robust far-field imaging by spatial coherence engineering. *Opto-Electron. Adv.* **2021**, *4*, 210027. [CrossRef]
20. Liu, Y.; Zhang, X.; Dong, Z.; Peng, D.; Chen, Y.; Wang, F.; Cai, Y. Robust far-field optical image transmission with structured random light beams. *Phys. Rev. Appl.* **2022**, *17*, 024043. [CrossRef]
21. Pan, R.; Liu, X.; Tang, J.; Ye, H.; Liu, Z.; Ma, P.; Wen, W.; Hoenders, B.J.; Cai, Y.; Liang, C. Enhancing the self-reconstruction ability of the degree of coherence of a light beam via manipulating the cross-phase structure. *Appl. Phys. Lett.* **2021**, *119*, 111105. [CrossRef]
22. Xu, Z.; Liu, X.; Chen, Y.; Wang, F.; Liu, L.; Monfared, Y.E.; Ponomarenko, S.A.; Cai, Y.; Liang, C. Self-healing properties of Hermite-Gaussian correlated Schell-model beams. *Opt. Express* **2020**, *28*, 2828–2837. [CrossRef] [PubMed]
23. Wang, F.; Chen, Y.; Liu, X.; Cai, Y.; Ponomarenko, S.A. Self-reconstruction of partially coherent light beams scattered by opaque obstacles. *Opt. Express* **2016**, *24*, 23735–23746. [CrossRef] [PubMed]
24. Broky, J.; Siviloglou, G.A.; Dogariu, A.; Christodoulides, D.N. Self-healing properties of optical Airy beams. *Opt. Express* **2008**, *16*, 12880–12891. [CrossRef] [PubMed]
25. Chu, X.; Zhou, G.; Chen, R. Analytical study of the self-healing property of Airy beams. *Phys. Rev. A* **2012**, *85*, 013815. [CrossRef]
26. Vetter, C.; Steinkopf, R.; Bergner, K.; Ornigotti, M.; Nolte, S.; Gross, H.; Szameit, A. Realization of Free-Space Long-Distance Self-Healing Bessel Beams. *Laser Photonics Rev.* **2019**, *13*, 1900103. [CrossRef]
27. Rasouli, S.; Khazaei, A.M.; Hebri, D. Radial carpet beams: A class of nondiffracting, accelerating, and self-healing beams. *Phys. Rev. A* **2018**, *97*, 033844. [CrossRef]
28. Ring, J.D.; Lindberg, J.; Mourka, A.; Mazilu, M.; Dholakia, K.; Dennis, M.R. Auto-focusing and self-healing of Pearcey beams. *Opt. Express* **2012**, *20*, 18955–18966. [CrossRef]
29. Wu, G.; Wang, F.; Cai, Y. Generation and self-healing of a radially polarized Bessel-Gauss beam. *Phys. Rev. A* **2014**, *89*, 043807. [CrossRef]

30. Bouchal, Z.; Wagner, J.; Chlup, M. Self-reconstruction of a distorted nondiffracting beam. *Opt. Commun.* **1998**, *151*, 207–211. [CrossRef]
31. Kaganovsky, Y.; Heyman, E. Wave analysis of Airy beams. *Opt. Express* **2010**, *18*, 8440–8452. [CrossRef]
32. Fahrbach, F.O.; Simon, P.; Rohrbach, A. Microscopy with self-reconstructing beams. *Nat. Photonics* **2010**, *4*, 780–785. [CrossRef]
33. Li, S.; Wang, J. Adaptive free-space optical communications through turbulence using self-healing Bessel beams. *Sci. Rep.* **2017**, *7*, 43233. [CrossRef]
34. Zhou, Y.; Wu, G.; Cai, Y.; Wang, F.; Hoenders, B.J. Application of self-healing property of partially coherent beams to ghost imaging. *Appl. Phys. Lett.* **2020**, *117*, 171104. [CrossRef]
35. Siviloglou, G.A.; Christodoulides, D.N. Accelerating finite energy Airy beams. *Opt. Lett.* **2007**, *32*, 979–981. [CrossRef]
36. Siviloglou, G.A.; Broky, J.; Dogariu, A.; Christodoulides, D.N. Observation of accelerating Airy beams. *Phys. Rev. Lett.* **2007**, *99*, 213901. [CrossRef]
37. Greenberger, D.M. Comment on "Nonspreading wave packets". *Am. J. Phys.* **1980**, *48*, 256. [CrossRef]
38. Zhu, Y.; Dong, Z.; Wang, F.; Chen, Y.; Cai, Y. Compact generation of robust Airy beam pattern with spatial coherence engineering. *Opt. Lett.* **2022**, *47*, 2846–2849. [CrossRef]
39. Hajati, M.; Sieben, V.; Ponomarenko, S.A. Airy beams on incoherent background. *Opt. Lett.* **2021**, *46*, 3961–3964. [CrossRef]
40. Liu, X.; Xia, D.; Monfared, Y.E.; Liang, C.; Wang, F.; Cai, Y.; Ma, P. Generation of novel partially coherent truncated Airy beams via Fourier phase processing. *Opt. Express* **2020**, *28*, 9777–9785. [CrossRef]
41. Sun, B.; Huang, Z.; Zhu, X.; Wu, D.; Chen, Y.; Wang, F.; Cai, Y.; Korotkova, O. Random source for generating Airy-like spectral density in the far field. *Opt. Express* **2020**, *28*, 7182–7196. [CrossRef]
42. Wen, W.; Mi, X.; Xiang, S. Quality factor of partially coherent Airy beams in a turbulent atmosphere. *J. Opt. Soc. Am. A* **2021**, *38*, 1612–1618. [CrossRef] [PubMed]
43. Baumgartl, J.; Mazilu, M.; Dholakia, K. Optically mediated particle clearing using Airy wavepackets. *Nat. Photonics* **2008**, *2*, 675–678. [CrossRef]
44. Jia, S.; Vaughan, J.C.; Zhuang, X. Isotropic three-dimensional super-resolution imaging with a self-bending point spread function. *Nat. Photonics* **2014**, *8*, 302–306. [CrossRef] [PubMed]
45. Vettenburg, T.; Dalgarno, H.I.; Nylk, J.; Coll-Lladó, C.; Ferrier, D.E.; Čižmár, T.; Gunn-Moore, F.J.; Dholakia, K. Light-sheet microscopy using an Airy beam. *Nat. Methods* **2014**, *11*, 541–544. [CrossRef]
46. Wang, J.; Hua, X.; Guo, C.; Liu, W.; Jia, S. Airy-beam tomographic microscopy. *Optica* **2020**, *7*, 790–793. [CrossRef]
47. Liang, Y.; Hu, Y.; Song, D.; Lou, C.; Zhang, X.; Chen, Z.; Xu, J. Image signal transmission with Airy beams. *Opt. Lett.* **2015**, *40*, 5686–5689. [CrossRef]
48. Zhu, G.; Wen, Y.; Wu, X.; Chen, Y.; Liu, J.; Yu, S. Obstacle evasion in free-space optical communications utilizing Airy beams. *Opt. Lett.* **2018**, *43*, 1203–1206. [CrossRef]
49. Ma, P.; Kacerovská, B.; Khosravi, R.; Liang, C.; Zeng, J.; Peng, X.; Mi, C.; Monfared, Y.E.; Zhang, Y.; Wang, F.; et al. Numerical approach for studying the evolution of the degrees of coherence of partially coherent beams propagation through an ABCD optical system. *Appl. Sci.* **2019**, *9*, 2084. [CrossRef]